Effects of Atmosphere on Slewing Control of a Flexible Structure

Jer-Nan Juang* and Lucas G. Horta†
NASA Langley Research Center, Hampton, Virginia

Air drag forces are introduced into the equations for a slewing control maneuver of a flexible structure to assess the effects of atmosphere on the controller design. Simulated modal parameters and transient responses are compared with experiments in normal atmosphere and vacuum. Analytical techniques for control laws are examined and verified. Physical insight into the air damping is gained so that results in vacuum can be extrapolated from results in air.

Introduction

In the past decade, a considerable volume of literature has been devoted to the problem of controlling the maneuvers of a system having flexible structural components. Optimal slewing control of a flexible structure is important in the control design of future industrial manipulators and a variety of space structures. Optimal slewing offers the improvement of manipulator performance and relaxation of the structural stiffness requirement imposed by conventional rigid body control techniques. Most research to date has been performed using computer simulations. A crucial step in the transition from mathematical simulation to the practical use of the technology is the demonstration of control design methodologies in the laboratory. References 1-6 are some examples of laboratory implementations that either validate theoretical control concepts for practical application or determine the reason for the difficulties and ineffectiveness of some control strategies. Research in Refs. 1-4 was performed to actively damp the vibrational motion of flexible structures. Investigators in Refs. 5 and 6 were interested in slewing a flexible structure and simultaneously damping induced vibrational motion at the end of the maneuver.

In all the tests discussed in Refs. 1-6, the time required for a controller to damp flexible motion was less than predicted in simulation, probably because the design model did not take into account air drag. The difference may be quite dramatic, particularly for large initial displacements with high velocities. Due to the lack of laboratory facilities, it may not be possible to test in vacuum. Studies to assess the effects of atmosphere become necessary to allow the extrapolation of results in vacuum from results in air. The system characteristics in orbit can then be predicted by analyzing the experimental results in normal atmosphere on the ground. The objective of this paper is to compare and measure differences between experimental results for the slewing control of a flexible panel in air and vacuum and to assess the effect of air drag on the controller design.

Presented as Paper 86-1001 at the AIAA/ASME/ASCE/AHS 27th Structures, Structural Dynamics, and Materials Conference, San Antonio, TX, May 19-21, 1986. Received June 16, 1986; revision received Oct. 20, 1986. Copyright © American Institute of Aeronautics and Astronautics, Inc. No copyright is asserted in the United States under Title 17, U.S. Code. The U.S. Government has a royalty-free license to exercise all rights under the copyright claimed herein for Governmental purposes. All other rights are reserved by the copyright owner.

*Senior Research Scientist, Structural Dynamics Branch. Associate Fellow.

†Aerospace Engineer, Structural Dynamics Branch. Member AIAA.

Hardware Setup

A 3.9-m-long flexible panel having a cross section of 0.64 m × 0.33 cm. is used for laboratory experiments in air and vacuum. The vacuum facility is a 15-m-diam thermovacuum chamber at the NASA Langley Research Center. The test model is cantilevered in a vertical plane and rotated in the horizontal plane by an electric gearmotor as shown in Fig. 1. The instrumentation consists of three full-bridge strain gages to measure bending moments induced by bending deformation and an angular potentiometer to measure the angle of rotation at the root. The strain gages are located at the root, at 22% of the panel length from the root, and at the midspan. Signals from all four sensors are amplified and then monitored by an analog data acquisition system. An analog computer closes the control loop, generating a voltage signal for the gearmotor based on an output feedback law.

Analysis: Dynamics and Control

The test apparatus is mathematically modeled as a flexible beam rotating about a vertical axis. The flexible beam is cantilevered from the motor at the root $x=0$ and free at the tip end $x=\ell$. By denoting EI the bending rigidity, ρ the mass density of the beam per unit length, y the bending deflection in the horizontal plane, and θ the root angle, the kinetic energy T and potential energy V can be expressed by (neglecting higher order terms)

$$2T=\int_0^\ell \rho(x\dot{\theta}+\dot{y})^2\mathrm{d}x=I_b\dot{\theta}^2+2\dot{\theta}\int_0^\ell \rho x\dot{y}\mathrm{d}x+\int_0^\ell \rho\dot{y}^2\mathrm{d}x \tag{1}$$

$$2V=\int_0^\ell EIy_{,xx}^2\mathrm{d}x \tag{2}$$

where $(\dot{}\,)=\mathrm{d}(\,)/\mathrm{d}t$, $(\,)_{,xx}=\partial^2(\,)/\partial x^2$, and $I_b=\int_0^\ell \rho x^2\mathrm{d}x$.

The generalized Hamiltonian principle is used to derive the equation of motion; i.e.,

$$\delta\int_{t_0}^{t_f}(T-V+W_{nc})\mathrm{d}t=0 \tag{3}$$

where W_{nc} is the work of the dissipative forces and t_0 and t_f represent the initial and terminal time, respectively.

When a thin plate rotates and vibrates transversely in air, various dissipative forces can cause free vibrations to decay. The dissipative forces can arise from external effects such as air drag and dissipation in the beam support or from internal characteristics of the beam material or structure. In this paper, the specific effect studied is the air drag. Some reasonable

comprehensive studies to date have been given in Ref. 7, reporting that one must consider two types of drag forces, namely one proportional to the instantaneous velocity and the other proportional to the square of the instantaneous velocity. Based on these reports, the drag forces per unit length on the beam slewing about a vertical axis can be written as

$$F_{D1} = C_1 (x\dot{\theta} + \dot{y})\, |x\dot{\theta} + \dot{y}| \tag{4}$$

and

$$F_{D2} = C_2 (x\dot{\theta} + \dot{y}) \tag{5}$$

where C_1 and C_2 are two coefficients to be specified. The coefficient C_1 is given in Ref. 8 as

$$C_1 = \tfrac{1}{2}\rho_a C_d W_s \qquad C_d = 5.63 S^{-1/5} \tag{6}$$

in which ρ_a is the air density, W_s is the width of the surface area S normal to the flow in square meters, and C_d is a dimensionless drag coefficient. The physical parameters entering C_2 are not clearly established, so this coefficient will merely be carried for completeness. Reference 8 shows that it is not clear from previous experiments whether the forces F_{D1} and F_{D2} are operable simultaneously at all velocities or there is a transition from F_{D1} to F_{D2} at some critical velocity. However, damping proportional to the velocity squared dominates at large amplitudes of motion.

Let the control torque τ be applied at the root of the beam. The virtual work produced by the control torque and the drag forces has the form of

$$\delta W_{nc} = -\tau\delta\theta + \int_0^\ell (F_{D1} + F_{D2})(x\delta\theta + \delta y)\,dx \tag{7}$$

The substitution of Eqs. (1), (2), and (7) into Eq. (3) yields the equations of motion

$$I_b\ddot{\theta} + \int_0^\ell \rho x\ddot{y}\,dx + \int_0^\ell C_1 (x\dot{\theta} + \dot{y})\, |x\dot{\theta} + \dot{y}|\, x\,dx + \int_0^\ell C_2 (x\dot{\theta} + \dot{y}) x\,dx = \tau \tag{8}$$

and

$$\rho\ddot{y} + \rho x\ddot{\theta} + C_1 (x\dot{\theta} + \dot{y})\, |x\dot{\theta} + \dot{y}| + C_2 (x\dot{\theta} + \dot{y}) + EIy_{,xxxx} = 0 \tag{9}$$

and the boundary conditions for a cantilever beam as

$$y(0,t) = y_{,x}(0,t) = y_{,xx}(\ell,t) = 0 \tag{10}$$

The set of equations (8–10) then constitutes equations of motion including air damping. The combined continuous and discrete system leads to nonlinear integrodifferential equations of motion that are difficult to solve analytically and even numerically; thus some simplification is helpful. For the case of a fast slew maneuver of the flexible beam, the instantaneous velocity $x\dot{\theta}$ due to the root angular velocity is usually one order of magnitude higher than the instantaneous velocity $\dot{y}$ due to the flexible bending. Based on this observation that $x\dot{\theta} \gg \dot{y}$ for all $\ell \geq x \geq 0$, Eqs. (8) and (9) can be reduced to

$$I_b\ddot{\theta} + \int_0^\ell \rho x\ddot{y}\,dx + \hat{C}_1\dot{\theta}\,|\dot{\theta}| + \hat{C}_2\dot{\theta} + \int_0^\ell C_2 \dot{y} x\,dx = \tau \tag{11}$$

and

$$\rho\ddot{y} + \rho x\ddot{\theta} + C_1 x^2\dot{\theta}\,|\dot{\theta}| + C_2(x\dot{\theta} + \dot{y}) + EIy_{,xxxx} = 0 \tag{12}$$

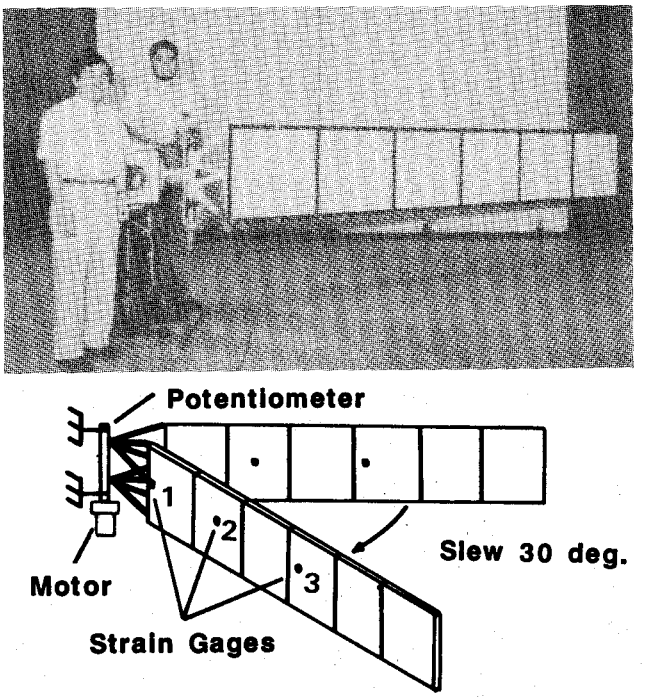

Fig. 1 Test setup of a slewing control experiment for a flexible panel.

where

$$\hat{C}_1 = C_1\ell^4/4; \qquad \hat{C}_2 = C_2\ell^3/3$$

To solve this set of nonlinear equations, consider the discretization

$$y(x,t) = \sum_{i=1}^{n} q_i(t)\phi_i(x) \tag{13}$$

in which n is the number of flexible modes included in the controller design, $q_i(t)$ are modal amplitudes, and $\phi_i(x)$ are shape functions satisfying the boundary conditions of Eq. (10). Introducing Eq. (13) into Eqs. (11) and (12), and applying the Rayleigh-Ritz method to Eq. (12), which minimizes the equation error, leads to an ordinary matrix differential equation

$$m\ddot{w} + d_a\dot{w} + kw = b\tau - f\dot{\theta}\,|\dot{\theta}| \tag{14}$$

where

$$w = (\theta, q_1, \ldots, q_n)^T$$

$$m = \begin{bmatrix} I_b & \int_0^\ell \rho x\phi_i(x)\,dx \\ \int_0^\ell \rho x\phi_j(x)\,dx & \int_0^\ell \rho\phi_i(x)\phi_j(x)\,dx \end{bmatrix}$$

i = column index = $1,\ldots,n$; j = row index = $1,\ldots,n$

$$d_a = \begin{bmatrix} \hat{C}_2 & \int_0^\ell C_2 x\phi_i(x)\,dx \\ \int_0^\ell C_2 x\phi_j(x)\,dx & \int_0^\ell C_2\phi_i(x)\phi_j(x)\,dx \end{bmatrix}$$

$$k = \begin{bmatrix} 0 & 0 \\ 0 & \int_0^\ell EI\phi_{i,xx}(x)\phi_{j,xx}(x)\,dx \end{bmatrix}$$

The vector b is null except for the first element $b_1 = 1$, and the vector f is given by

$$f = \left[\hat{C}_1, \int_0^\ell C_1 x^2 \phi_1(x)\mathrm{d}x, \ldots, \int_0^\ell C_1 x^2 \phi_n(x)\mathrm{d}x\right]^T$$

For the case where $C_1 = 0$, the vector f become null and Eq. (14) reduces to a linear matrix equation that includes only air drag proportional to velocity.

The actuator dynamics and sensor characteristics used in conjunction with Eq. (14) were fully described in Ref. 5. For the sake of completeness, a brief description is as follows.

The actuator located at the root of the beam is a direct current electric motor with a gear train and electromechanical brakes modified for vacuum application. The electric motor is modeled as a standard armature circuit. Denote the armature resistance by R_a, the back-EMF (electro-motive-force) constant by k_b, the motor torque constant by k_t, the motor inertia by I_m, the gear train viscous drag coefficient by C_b, and the overall gear ratio by N_g. The torque τ produced by the actuator can be expressed by

$$\tau = (N_g k_t / R_a) e_a - (k_t k_b / R_a + C_v) N_g^2 \dot{\theta} - I_m N_g^2 \ddot{\theta} \qquad (15)$$

where e_a is the applied voltage (command signal) to the armature and θ is the root angle.

The angle is measured by a rotary potentiometer, whereas the bending moment is measured by strain gages. Let c_p be the conversion factor between the root angle θ and the output voltage e_p of the potentiometer and c_s be the conversion factor between the strain and the strain gage output voltage e_o. If there are three strain gages distributed along the beam located at x_1, x_2, and x_3, an output measurement equation can be written in matrix form as

$$e = \begin{bmatrix} e_p \\ e_o(x_1) \\ e_o(x_2) \\ e_o(x_3 \end{bmatrix} = \begin{bmatrix} c_p & 0 \\ 0 & c_\epsilon \end{bmatrix} w \qquad (16)$$

where

$$c_\epsilon = c_s \begin{bmatrix} \phi_{1,xx}(x_1), \ldots, \phi_{n,xx}(x_1) \\ \phi_{1,xx}(x_2), \ldots, \phi_{n,xx}(x_2) \\ \phi_{1,xx}(x_3), \ldots, \phi_{n,xx}(x_3) \end{bmatrix}$$

The coefficients of the matrix can be determined by inserting the assumed shape functions. This equation relates the output voltage e to the root angle θ and the generalized coordinates q_i. An active controller can then be designed using Eqs. (15) and (16).

Now let $k_g \triangleq [k_p, k_1, k_2, k_3]^T \triangleq [k_p, k_o^T]^T$ be the gain vector for the output measurement e such that the applied voltage e_a (command signal) to the gearmotor in Eq. (15) is given by

$$e_a = k_g^T e = -k_p e_p - k_1 e_o(x_1) - k_2 e_o(x_2) - k_3 e_o(x_3)$$
$$= [k_p c_p, k_o^T c_\epsilon] w \qquad (17)$$

This is the output feedback law. No velocity feedback is included in Eq. (17) because the motor back-EMF provides sufficient damping, which is shown in the following equations. Substituting Eqs. (15) and (17) into Eq. (14) yields a closed-loop equation of motion in matrix form as

$$\bar{m}\ddot{w} + \bar{d}\dot{w} + \bar{k}w = -f\dot{\theta}\,|\dot{\theta}| \qquad (18)$$

where

$$\bar{m} = m + \begin{bmatrix} I_m N_g^2 & 0 \\ 0 & 0 \end{bmatrix}$$

$$\bar{d} = d_a + \begin{bmatrix} (k_t k_b / R_a + C_v) N_g^2 & 0 \\ 0 & 0 \end{bmatrix}$$

$$\bar{k} = k + \begin{bmatrix} k_p c_p & k_0^T c_\epsilon \\ 0 & 0 \end{bmatrix} (N_g k_t / R_a)$$

m, d_a, and k are defined in Eq. (14).

Equation (18) is the fundamental equation of motion, including air damping, for a beam rotating about a vertical axis. When the system is in vacuum, the linear damping matrix d_a and the nonlinear damping vector f in Eq. (18) become null. The equation of motion thus reduces to a simple linear matrix form by which closed-loop system eigenvalues can be computed.

In order to shape the control torque to minimize the excitation of vibrational motion, a differential equation describing the torque profile should be augmented to the state equation. Instead of Eq. (17), let the torque equation in terms of the applied voltage e_a (command signal) be given by

$$\dot{e}_a = C_\tau e_a + e_{a_1} \qquad (19)$$

where C_τ is the torque shaping constant for the torque profile and e_{a_1} is a new feedback control variable. Note that this is referred to as a first-order filter equation. Now using the notation of the gain vector in Eq. (17), assume that the feedback control variable e_{a_1} is determined by

$$e_{a_1} = -[k_w^T, k_e] \begin{bmatrix} w \\ e_a \end{bmatrix}; \quad k_w^T = [k_p c_p, k_0^T c_\epsilon] \qquad (20)$$

Here k_e is a gain constant for the applied voltage e_a to the motor. The substitution of Eq. (20) into Eq. (19) and Eq. (15) into Eq. (14) yields closed-loop equations of motion in the following matrix form:

$$\bar{m}\ddot{w} + \bar{d}\dot{w} + kw = be_a N_g K_t / R_a - f\dot{\theta}\,|\dot{\theta}| \qquad (21)$$

$$\dot{e}_a + (k_e - C_\tau) e_a + k_w^T w = 0 \qquad (22)$$

where the matrices $\bar{m}$, $\bar{d}$, and k are defined in Eqs. (14) and (18).

Table 1 Model parameters

Motor	Strain gages
$k_t = .0297$ n-m/A	$G = 2.115$
$k_b = 0.0296$ V-s/rad	$e_i = 5.0$ V
$R_a = 4.1\ \Omega$	Atmosphere[6]
$L_a = 10$ mh	$\rho_a = 1.1595$ N s^2/m^4
$I_m = 4.02 \times 10^6$ n-m-s^2	$C_1 = 2.78$
$N_g = 941$	$C_2 = 0.$

Flexible panel (aluminum/honeycomb)

$\ell = 3.9$ m
$EI = 328.3$ n-m^2
$\rho = 3.08$ kg/m
$h = 0.65$ cm

Conversion factors (machine units)

$c_p = 0.17$ V/rad
$c_s = 2.64$ V/m/m

Table 2 Controller design gains for flexible panel (Ref. 5)

Control law	$e_a = k_p e_p + k_1 e_o(x_1) + k_2 e_o(x_2) + k_3 e_o(x_3)$
Gain constants	$k_p = -43.48 \quad k_1 = 6.5 \quad k_2 = 11.8 \quad k_3 = 0.06$
Torque shaping constant	$C_\tau - k_e = -6.5$

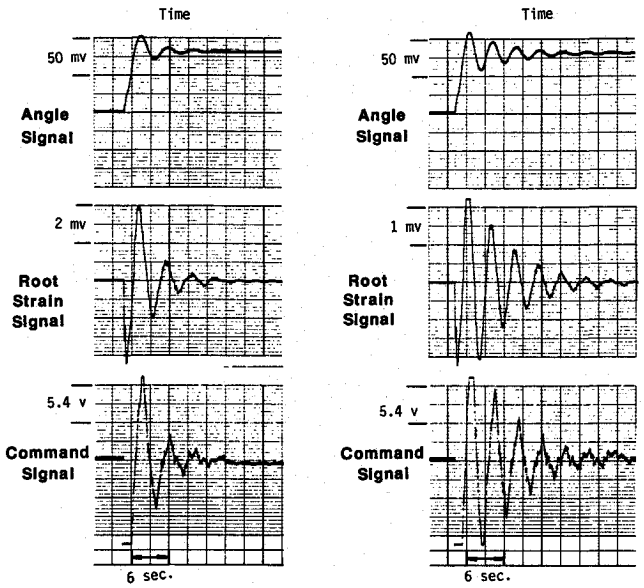

a) in air b) in vacuum

Fig. 2 Time responses from the slewing control experiment.

Equation (22) provides the freedom to choose the initial applied voltage $e_a(0)$, which usually is set to zero to minimize the excitation of high-frequency modes due to the torque discontinuity at the initial time. It will be shown in the following sections that Eq. (19) in conjunction with the feedback equation [Eq. 20)] provides smooth torque profiles that not only minimizes the excitation of the high-frequency modes but also reduces the effects of system nonlinearities and uncertainties such as deadband and backlash. To smooth the torque profile further, a differential equation of higher order than Eq. (19) can be defined to allow the choices of initial applied voltage e_a and initial voltage derivatives $d^i e_a/dt^i$ $(i=1,2,...)$. Note that several different approaches have been developed and demonstrated for control profile shaping (see Refs. 9 and 10).

Experimental Results

Table 1 shows the electric motor, strain gage and flexible panel parameters, and conversion factors used in the feedback control law design, whereas Table 2 gives the control gains defined in Eqs. (17) and (20). Figures 2a and 2b show different time response curves of the angle signal e_p, the root strain signal e_o, and the torque command signal e_a for the panel experiments performed in air at normal atmospheric pressure and in near vacuum (4 mm Hg). These curves are directly obtained from the analog plotter. The flexible panel, as shown in Fig. 1, is slewed about 30 deg. The angle signal is measured relative to a reference signal, which is given initially to initiate the control maneuver. The command signal transmitted to the gearmotor is computed by feeding back the strain signals measured from the strain gages and the rotation angle signal from the potentiometer [see Eq. (17)]. The rotational angle and three lowest flexible bending modes are used to represent the panel dynamics. The time to damp the motion in air (Fig. 2a) is about one-half less than that in vacuum (Fig. 2b). This higher damping rate is due to air drag.

Table 3 Comparison of analytical predictions with experimental results

		Air		Vacuum	
	Mode	Frequency, Hz	Damping, %	Frequency, Hz	Damping, %
Analysis	1	0.28	8.4	0.28	3.7
	2	2.03	6.6	2.04	6.6
	3	5.99	2.0	5.99	2.0
Experiment	1	0.25	13.9	0.27	8.6
	2	2.21	0.5	2.45	0.4
	3	[a] –	–	–	–
Analysis[b]	1	0.22	36.6	0.22	33.6
	2	2.13	6.9	2.14	6.4
	3	6.00	1.4	6.00	1.6
Experiment[b]	1	0.24	28.9	0.23	32.4
	2	2.14	1.5	2.49	1.6
	3	–	–	–	–

[a]Unable to identify. [b]With torque shaping.

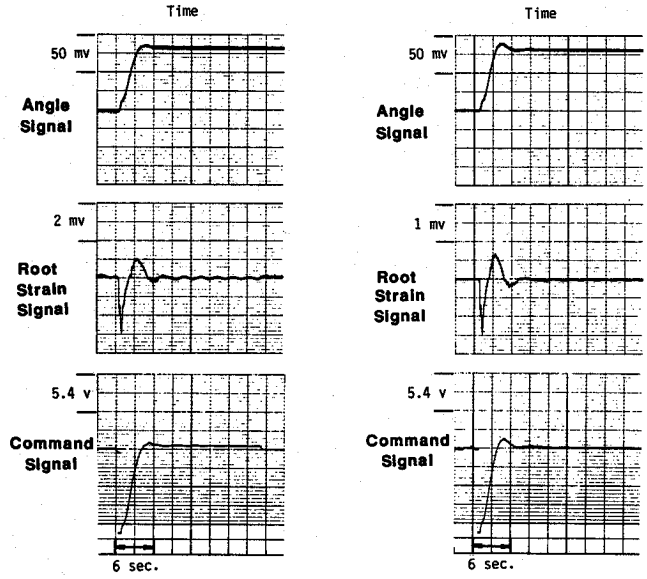

a) in air b) in vacuum

Fig. 3 Time responses from the slewing control experiment with torque shaping.

Now consider a controller design including a first-order filter to shape the feedback command signal [see Eq. (19)] so as to provide a high damping ratio for the first mode and minimize the excitation of high-frequency modes. The time responses of the angle signal, the root strain signal, and the command signal are shown in Figs. 3a and 3b for experiments in air and vacuum respectively. The panel is slewed about 30 deg in 4 s. The time to slew the panel in vacuum, shown in Fig. 3b, is less than that shown in Fig. 3a because there is no air resistance during the maneuver. The vibrational motion in this case is minimized so that air drag plays a minimum role in providing damping. It is shown that the effect of air drag on the damping values for vibrational motion in a slewing control maneuver depends on the controller design.

Comparison of Theory and Experiment

Only two strain signals, located at the root and 22% of the beam length, are recorded in all of the experiments for transient analysis and modal parameter identification. Since both strains behave in a similar manner, only the root strain signal will be shown to illustrate the comparison of the analytical simulation with the experimental results. Figure 4 shows the results for 30-deg maneuvers in air and vacuum. The solid line

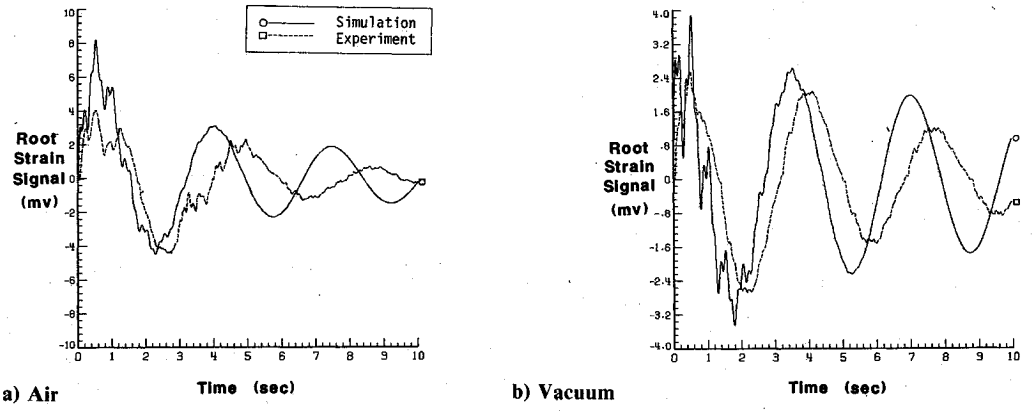

Fig. 4 Transient responses for simulated and experimental data for a 30-deg maneuver.

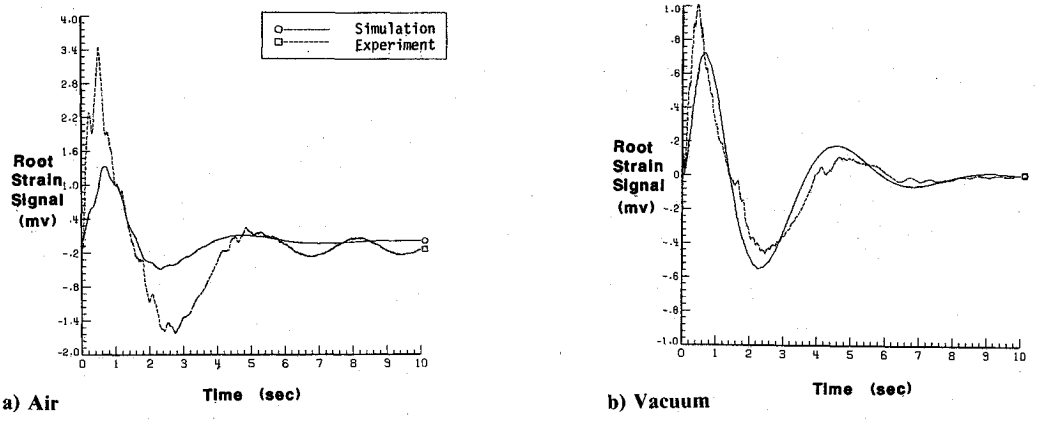

Fig. 5 Transient responses for simulated and experimental data for a 30-deg maneuver with torque shaping.

represents simulation data, whereas the dashed line represents the experimental data. Similar trends are observed in the transient responses. The ordinate is in millivolts, which can be converted to strain by using the conversion factor c_s. During the slewing maneuver, the root end of the panel has zero velocity, but the free end has maximum velocity. Therefore, the analytical simulation in air uses the nonlinear drag coefficent $C_1 = 2.78$, which is an average value for the panel cantilevered at the rotating axis.

The predicted and experimental frequencies and damping values are shown in Table 3. In addition to the transient analysis, the laboratory data was analyzed using the Eigensystem Realization Algorithm (ERA).[11,12] Since the system dynamics including air damping are nonlinear, the data length must be considered in the interpretation of modal parameters. However, examination of modal parameters identified using several different data lengths indicates that no significant variation of results occurs. Harmonic frequencies reflecting nonlinearities of the system dynamics do appear.[13] As a result, the dynamic behavior for those cases in air can be approximately described by the modal parameters. The slewing maneuvers designed for this experiment excited primarily the first mode. Because the second and third modes are not significantly excited by the maneuvers, their corresponding dampings and frequencies are not considerably affected by the air. Therefore, the predicted dampings and frequencies shown in Table 3 are the same whether in air or vacuum. The predicted first-mode frequency in air (Fig. 4a, Table 3) is 13% lower than measured in the experiment. This is because of the softening effect of the gear train backlash that is not properly modeled if cantilever modes are used in the beam discretization. The same phenomena in vacuum is shown in Fig. 4. The experimental result for the first mode shows a decrease in damping by a factor of 1.6 whereas the analysis predicts a factor of 2.3. In both cases (in air and in vacuum), the analytically predicted damping values for the first mode are lower than those in the experiment. The difference for the first mode is attributed to the dissipative effect of the gear train backlash not modeled. A reduction of the peak strain signal is also observed in vacuum because no air opposes the maneuver.

Figure 5 shows the results for the same maneuver in air and vacuum when the command signal profile is shaped according to Eqs. (21) and (22). The corresponding frequencies and damping values are also shown in Table 3. In vacuum, the first-mode frequency and damping are within 5% of the predicted values. Thus good agreement is observed in the transient analysis. The experimental data in air (Fig. 5a) depict a residual motion caused by air circulation in the laboratory while conducting the experiment. The predicted frequency for the first mode is within 8% of the experimental values, but damping differs by almost 40%. This discrepancy results in an underestimation of the peak strain values as shown in Fig. 5a. With the exception of the peak strain signals, the trends of the curves in Fig. 5a agree reasonably. It is believed that the gear-train backlash and deadband effects contribute significantly to the increase of the peak strain value when air is opposing the slew maneuver, particularly for the case with torque shaping. The discrepancy is also attributed to modeling errors of the drag forces. The drag coefficient C_d as shown in Eq. (6) is generally a function of vibration amplitude.

In general, the virtual mass effect should be included in the equations of motion for the flexible panel. The air inertia primarily affects the natural frequencies of the system,[8] whereas the air drag affects the damping. However, the results in Table 3 show good agreements in frequencies, which suggests that the discrepancies between analysis and experiment are not attributed to the virtual mass effects.

Conclusions

In this paper, the effects of atmosphere on the slewing control of a flexible panel is investigated by including air damping terms in the differential equations for an angular rotation coupled with beam vibration. The prediction of transient responses, frequencies, and damping ratios is compared with

experimental results. Based on these comparisons, the following conclusions are drawn:

1) Damping effects due to atmosphere can be systematically and effectively included in the equations for the slewing maneuvers of a flexible panel. By using the analysis technique shown here, one can include air damping in the numerical simulation to extrapolate the characteristics of the system in vacuum.

2) Torque shaping makes significant changes in the system performance. The agreement between analysis and experiment is improved when torque shaping is used. Nonlinearities are minimized because the number of system modes excited are minimum. Particular high-frequency modes are hardly excited.

3) The significance of air damping effects depends on the controller design for flexible structures. The smoother the controller is, the less the effects of air damping will be.

4) System uncertainties and nonlinearities can also contribute to the effects of air damping on the transient responses. For example, the deadband in the actuator may significantly increase the amplitude of the vibrational motion for a specific controller design.

References

[1]Schaechter, D.B., "Hardware Demonstration of Flexible Beam Control," *Journal of Guidance, Control, and Dynamics,* Vol. 5, Jan.-Feb. 1982, pp. 48–52.

[2]Hallauer, W.L. Jr., Skidmore, G.R., and Gehling, R.N., "Modal-Space Active Damping of a Plane Grid: Experiment and Theory," *Journal of Guidance, Control, and Dynamics,* Vol. 8, May–June 1985, pp. 366–373.

[3]Bauldry, R.D., Breakwell, J.A., Chambers, G.J., Johansen, K.F, Nguyen, N.C., and Schaechter, D.B., "A Hardware Demonstration of Control for a Flexible Offset-Feed Antenna," *The Journal of the Astronautical Sciences,* Vol. 31, July–Sept. 1983, pp. 455–470.

[4]Meirovitch, L., Baruh, H., Montgomery, R.C., and Williams, J.P., "Nonlinear Natural Control of an Experimental Beam," *Journal of Guidance, Control, and Dynamics,* Vol. 7, July–Aug. 1984, 1984, pp 437–442.

[5]Juang, J.-N., Horta, L.G., and Robertshaw, H., "A Slewing Control Experiment for Flexible Structures," *Journal of Guidance, Control, and Dynamics,* Vol. 9, Sept.-Oct. 1986, pp. 599–607.

[6]Alberts, T.E., "Augmenting the Control of a Flexible Manipulator with Passive Mechanical Damping," Ph.D. dissertation, Georgia Institute of Technology, Atlanta, GA, Sept. 1986.

[7]Baker, W.E., Woolam E., and Young, D., "Air and Internal Damping of Thin Cantilever Beams," *International Journal of Mechanical Sciences,* Vol. 9, Nov. 1967, pp. 743–766.

[8]Woolam, E.W., "Drag Coefficients for Flat Square Plates Oscillating Normal to Their Planes in Air," NASA CR-66544, March 1968, AIAA Paper 78-1692, Sept. 1978.

[9]Swigert, C.J., "Shaped Torques Technique," AIAA Paper 78-1692, Sept. 1978.

[10]Gupta, N.K., Lyons, M.G., Aubrun, J.N., and Margulies, G., "Frequency-Shaping Methods in Large Space Structures Control," AIAA Paper 81-1783, Aug. 1981.

[11]Juang, J.-N. and Pappa, R.S., "An Eigensystem Realization Algorithm for Modal Parameter Identification and Modal Reduction," *Journal of Guidance, Control, and Dynamics,* Vol. 8, Sept.-Oct. 1985, pp. 620–627.

[12]Juang, J.-N. and Pappa, R.S., "Effects of Noise on Modal Parameters Identified with the Eigensystem Realization Algorithm," *Journal of Guidance, Control, and Dynamics,* Vol. 9, May–June 1986, pp. 294–303.

[13]Horta, L.G. and Juang, J.N., "Identifying Approximate Linear Models for Simple Nonlinear Systems," *Journal of Guidance, Control, and Dynamics,* Vol. 9, July–Aug. 1986, pp. 385–390.